JOURNAL OF MATERIALS SCIENCE 28 (1993) 2299–2303

Room temperature deformation modes in DO_3-structured Fe–34Al and Fe–28Al–6Cr

P. R. MUNROE
School of Materials Science and Engineering, University of New South Wales, Kensington, NSW 2033, Australia

I. BAKER
Thayer School of Engineering, Dartmouth College, Hanover, NH 03755, USA

The dislocation substructures in the DO_3-structured alloys, Fe–34Al and Fe–28Al–6Cr, were examined by transmission electron microscopy following room temperature compression. In both alloys a small number of a⟨0 0 1⟩ dislocations, produced through the energetically favourable interaction of two pairs of antiphase boundary-coupled $a/2\langle 1\,1\,1\rangle$ dislocations, was observed. It was also found that, relative to the binary alloy, one effect of the chromium addition was to increase the B2 character of the alloy, but conversely to decrease the DO_3 character. These results are rationalized on the basis of the atom site location of the chromium atoms in the DO_3 structure.

1. Introduction

B2-structured FeAl, containing less than ~ 38% Al (compositions are given throughout in atomic per cent), may undergo ordering of second nearest neighbours to form a DO_3 (Fe_3Al) structure [1]. For aluminium contents between 25% and 38%, the temperature at which this transformation occurs increases as the aluminium content decreases. Schematic diagrams of both the B2 and DO_3 structures are shown in Fig. 1. The lattice parameter, a', of the DO_3 unit cell is twice that of the B2 unit cell lattice parameter, a. In B2-structured FeAl, slip occurs through the motion of a pair of anti-phase boundary, APB-coupled, $a/2\langle 1\,1\,1\rangle$ dislocations [2–8], whereas in compositions at, or near to, stoichiometric Fe_3Al, slip occurs through the movement of a unit dislocation consisting of four $a'/4\langle 1\,1\,1\rangle$ dislocations (Fig. 1c) [9]. The four-fold dislocations are coupled by two types of APB. The outer pairs by an APB (energy per unit area γ_1) arising from the first nearest-neighbour interactions, and the inner pair by an APB (with energy per unit area γ_2) affected by second nearest-neighbour interactions. As the aluminium content increases, γ_1 increases and the separation R_1 decreases, whilst γ_2 decreases and the separation R_2 increases [10].

In a study of DO_3-structured Fe–34Al, only $a'/4\langle 1\,1\,1\rangle$ APB (γ_1) dislocation pairs were observed. The partials were ~ 4.5 nm apart, from which an APB energy, γ_1, of 110 $J\,m^{-2}$ was calculated, using anisotropic elasticity theory [10]. No four-fold dissociations were observed but it was suggested that γ_2 was so low that the separation R_2 was large enough for the two APB (γ_1)-coupled dislocation pairs to become uncoupled and glide independently. Recently, McKamey *et al.* [11] studied a range of DO_3-structured ternary alloys, based upon the composition Fe–28Al + Cr, where the chromium content varied between 0% and 6%. The APB spacings were measured only for Fe–28Al and Fe–28Al–4Cr, and it was shown that the chromium addition increased both R_1 and R_2.

A study of iron-rich, B2-structured Fe–34Al showed that during room-temperature deformation two APB-coupled ⟨1 1 1⟩ screw dislocation pairs can interact to form two near-edge $a\langle 0\,0\,1\rangle$ dislocations [8]. It was suggested that the presence of these ⟨0 0 1⟩ dislocations may be a cause of transgranular fracture on {0 0 1}. ⟨0 0 1⟩ dislocations were not reported in the DO_3-structured alloys described above.

This paper describes the dislocation structures of both DO_3-structured Fe–34Al and Fe–28Al–6Cr following room-temperature compression. The structures are compared with the dislocation structures of the above B2-structured Fe–34Al, DO_3-structured stoichiometric Fe_3Al and DO_3-structured Fe–28Al–Cr alloys.

2. Experimental procedure

The processing route for the Fe–34Al has been described elsewhere [12]. Fe–34Al samples were annealed at 1123 K for 1 h (this removed the residual dislocations resulting from prior processing), and water-quenched, to retain the B2 structure. In order to produce the DO_3 structure, samples were then annealed at 633 K for 100 h. The processing route of the Fe–28Al–6Cr has been described elsewhere [11]. In this study, hot-rolled strips, ~ 750 μm thick, of Fe–28Al–6Cr were heat treated at 1123 K for 1 h, water quenched and aged at 773 K for 100 h.

In order to introduce dislocations, cylinders ~ 10 mm × 3 mm of Fe–34Al were strained ~ 1% in

0022–2461

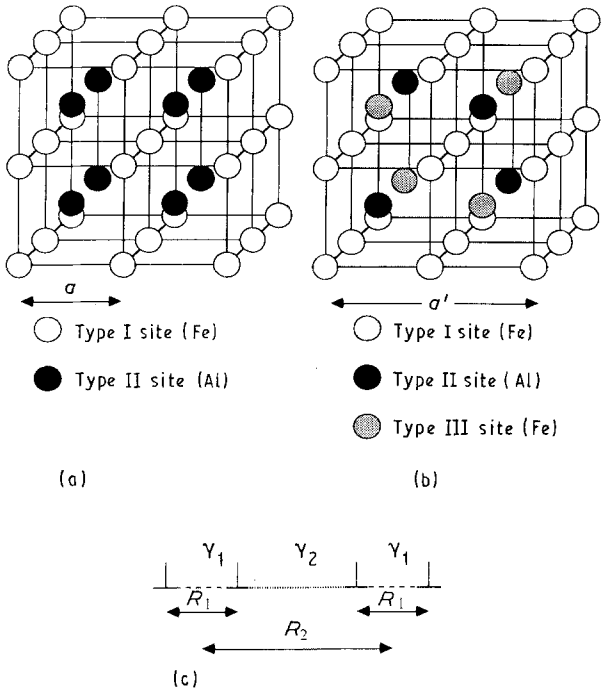

Figure 1 Schematic diagrams of (a) the B2 structure, (b) the DO_3 structure, (c) a unit DO_3 type superlattice dislocation; see text for details.

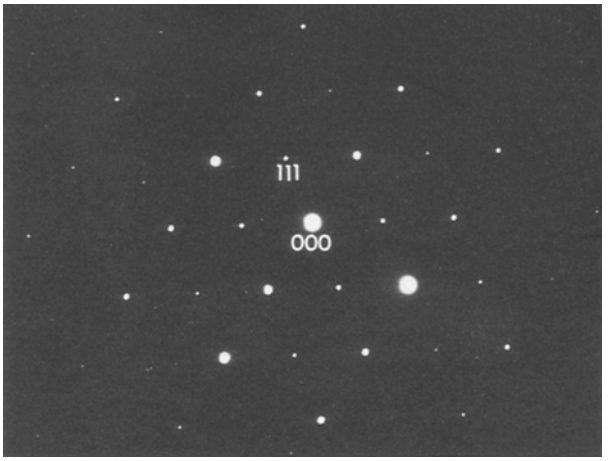

Figure 2 Selected-area diffraction pattern from ⟨1 1 0⟩ zone axis in DO_3-structured Fe–34Al; note the presence of the DO_3 reflections.

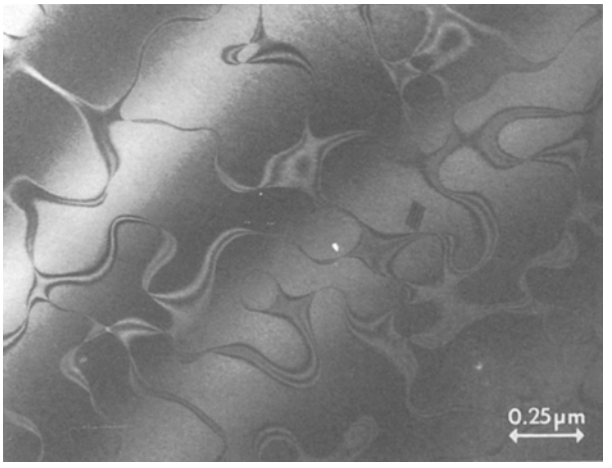

Figure 3 Bright-field electron micrograph showing APB contrast from Fe–28Al–6Cr, annealed at 1123 K for 1 h, water quenched and then annealed at 773 K for 100 h.

compression at a strain rate of $\sim 10^{-4}\,s^{-1}$ at room temperature. The strips of Fe–28Al–6Cr were rolled lightly, at room temperature, to $\sim 2\%$ strain. Thin foils were prepared from the strained alloys in a manner described elsewhere [11, 13] and examined in a Jeol 2000FX transmission electron microscope (TEM) operating at 200 kV. Dislocation analyses were performed using the $\boldsymbol{g}\cdot\boldsymbol{b} = 0$ invisibility criterion [14] for two-beam conditions, where $\boldsymbol{g}$ is the operating reflection and $\boldsymbol{b}$ is the Burgers' vector.

3. Results

A selected-area diffraction (SAD) pattern from a ⟨1 1 0⟩ zone axis in DO_3-structured Fe–34Al is shown in Fig. 2. {1 1 1} DO_3 superlattice reflections can be clearly observed in the DO_3 pattern, although these reflections are less intense than either the fundamental reflections or the B2 superlatice reflections. In earlier studies, no {1 1 1} DO_3 superlattice reflections were observed at a ⟨1 1 0⟩ zone axis pattern from B2-structured Fe–34Al [8].

It is worth noting that in X-ray diffraction studies of Fe–34Al which had been heat treated to stabilize the DO_3 structure, DO_3 superlattice reflections were not observed; indeed it was concluded that the B2 and DO_3 structures of Fe–34Al were indistinguishable by this means [15]. This was confirmed by X-ray diffractometry of Fe–34Al, in both the B2 and DO_3 states, conducted as part of this study. That DO_3 superlattice reflections are observed in this alloy for electron diffraction, suggests that it does have some DO_3 character, however slight. Similar {1 1 1} DO_3 superlattice reflections were observed in SAD patterns from Fe–28Al–6Cr. No APBs were observed in Fe–34Al, but APBs were observed in Fe–28Al–6Cr (Fig. 3).

The dislocation substructure of DO_3-structured Fe–34Al strained in compression at room temperature is shown in Fig. 4. No four-fold dislocations were observed. The majority of the dislocations observed consisted of APB-coupled ⟨1 1 1⟩ dislocations: for example, the dislocations marked *a* in Fig. 4 show either invisibility or residual contrast when $\boldsymbol{g} = 1\,1\,0$ and $\boldsymbol{g} = \bar{1}\,0\,1$, indicating that $\boldsymbol{b} = [1\,\bar{1}\,1]$. FeAl is strongly anisotropic. The Zener anisotropy factor, *A*, of Fe–34Al is 4.4 [16], and there is usually residual contrast even when a screw dislocation is viewed under conditions which satisfy the $\boldsymbol{g}\cdot\boldsymbol{b} = 0$ invisibility criterion. Trace analyses were used to show that the ⟨1 1 1⟩ dislocations are screw in character.

In addition to the APB-coupled ⟨1 1 1⟩ dislocations described above, dislocations such as *b* were observed; this shows invisibility when $\boldsymbol{g} = 0\,\bar{2}\,0$ and weak contrast when $\boldsymbol{g} = 0\,1\,\bar{1}$, indicating that $\boldsymbol{b} = [1\,0\,0]$. The line direction of this dislocation was found by trace analysis to be [0 1 0], indicating that the dislocation *b* is edge in character. Further analysis was performed using the $\boldsymbol{g}\cdot\boldsymbol{b}\times\boldsymbol{u} = 0$ invisibility criterion for edge dislocations. For the dislocation *b*, $\boldsymbol{b}\times\boldsymbol{u} = [0\,0\,1]$.

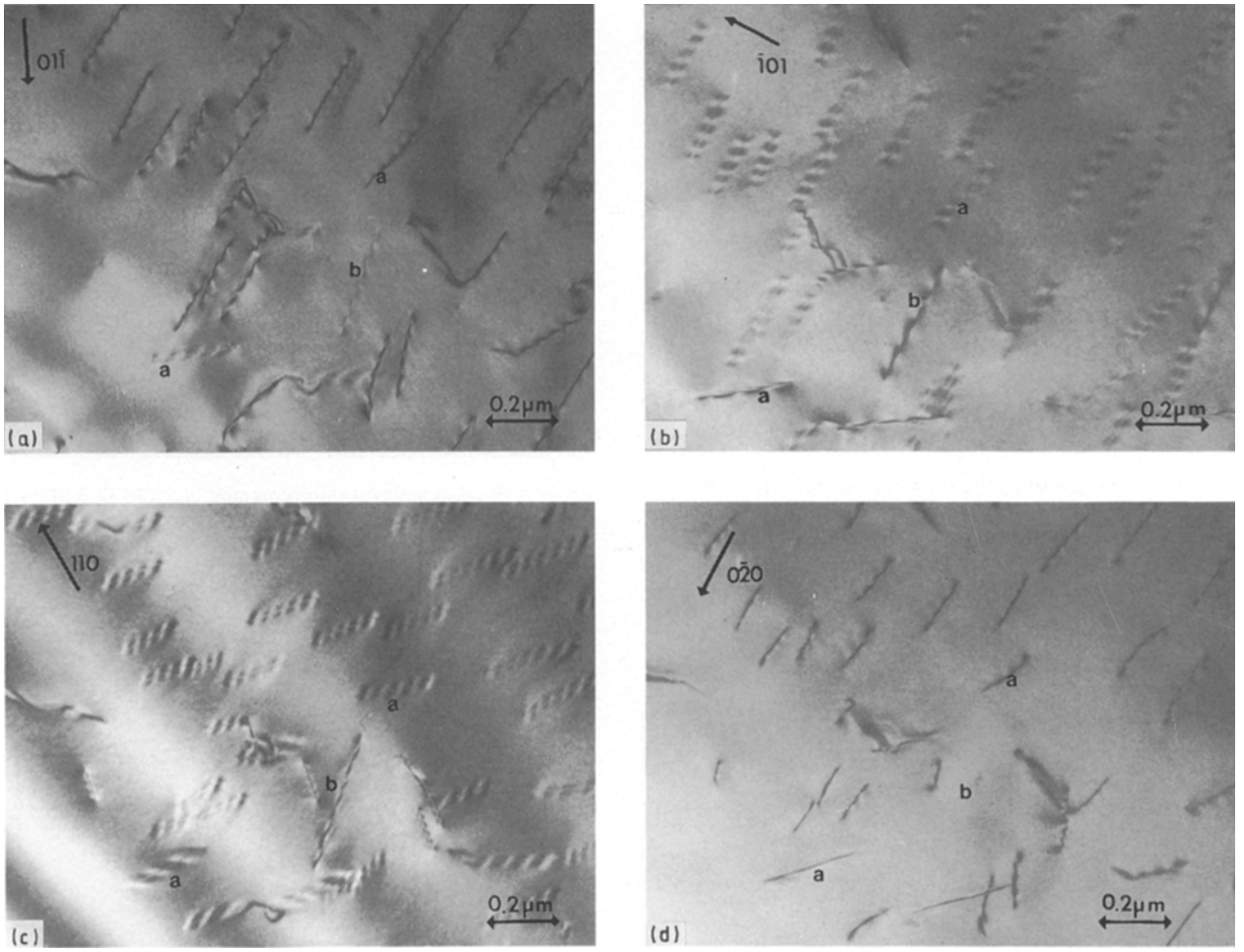

Figure 4 Dislocation substructure from DO_3-structured Fe–34Al, strained in compression at room temperature. The dislocations labelled *a* exhibit contrast consistent with a $[1\,\bar{1}\,1]$ Burgers' vector. The dislocation labelled *b* exhibits contrast consistent with a [1 0 0] Burgers' vector. Diffraction vectors as shown, beam directions for (a) and (b) close to [1 1 1], (c) and (d) close to [0 0 1].

Therefore, at $\boldsymbol{g} = 0\,\bar{2}\,0$ $\boldsymbol{g}\cdot\boldsymbol{b} = 0$ and $\boldsymbol{g}\cdot\boldsymbol{b}\times\boldsymbol{u} = 0$ indicating complete invisibility, but when $\boldsymbol{g} = 0\,1\,\bar{1}$ $\boldsymbol{g}\cdot\boldsymbol{b} = 0$ but $\boldsymbol{g}\cdot\boldsymbol{b}\times\boldsymbol{u} = 1$, indicating weak residual contrast consistent with the contrast observed in Fig. 4. In B2-structured Fe–34Al, pairs of ⟨0 0 1⟩ dislocations were observed [8]. Although in the example provided, only a single ⟨0 0 1⟩ dislocation was observed, ⟨0 0 1⟩ dislocation configurations similar to those seen in B2-structured Fe–34Al, were also observed in this alloy (Fig. 5). It is interesting to note that the ⟨1 1 1⟩ dislocations exhibit a distinctive "double-dotted" contrast when they satisfy the invisibility criterion, whereas ⟨0 0 1⟩ dislocations exhibit little residual contrast when $\boldsymbol{g}\cdot\boldsymbol{b} = 0$ is satisfied. Similar "double-dotted" contrast is exhibited by ⟨1 1 1⟩ screw dislocations in both NiAl [17] and β-brass [18] when $\boldsymbol{g}\cdot\boldsymbol{b} = 0$ is satisfied.

Dislocation structures, similar to those observed in Fe–34Al, were also observed in Fe–28Al–6Cr. Fig. 6 shows a typical dislocation structure, APB-coupled ⟨1 1 1⟩ dislocations can be seen labelled *a*, together with a ⟨0 0 1⟩ dislocation labelled *b*. Again, no four-fold dislocations were observed.

Fig. 7 shows a weak-beam electron micrograph of a pair of APB (γ_1)-coupled ⟨1 1 1⟩ dislocations in Fe–34Al, which have a separation ~ 5 nm. This spacing is consistent with that observed between APB (γ_1)-coupled ⟨1 1 1⟩ dislocations in B2-structured Fe–34Al [4] and is equivalent to an APB energy of ~ 110 mJ m^{-2} [10]. Similarly, weak-beam imaging of Fe–28Al–6Cr indicated APB (γ_1)-coupled ⟨1 1 1⟩ dislocations separated by ~ 10 nm equivalent to a APB

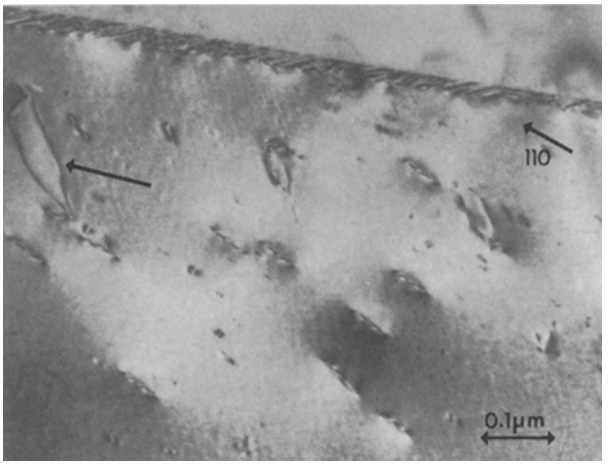

Figure 5 Bright-field transmission electron micrograph from DO_3-structured Fe–34Al, strained in compression at room temperature showing ⟨0 0 1⟩ dislocation pair (arrowed), similar to those previously observed in B2-structured Fe–34Al (see [8]). Diffraction vector as shown, $B \sim [0\,0\,1]$.

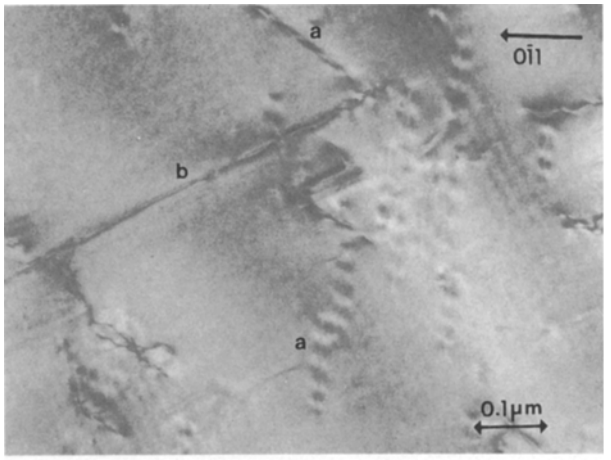

Figure 6 Dislocation substructure from DO_3-structured Fe–28Al–6Cr, lightly rolled at room temperature. Dislocations marked *a* exhibit contrast consistent with a ⟨1 1 1⟩ Burgers' vector while the dislocation labelled *b* exhibits contrast consistent with a ⟨0 0 1⟩ Burgers' vector. Diffraction vector as shown, beam direction close to [1 1 1].

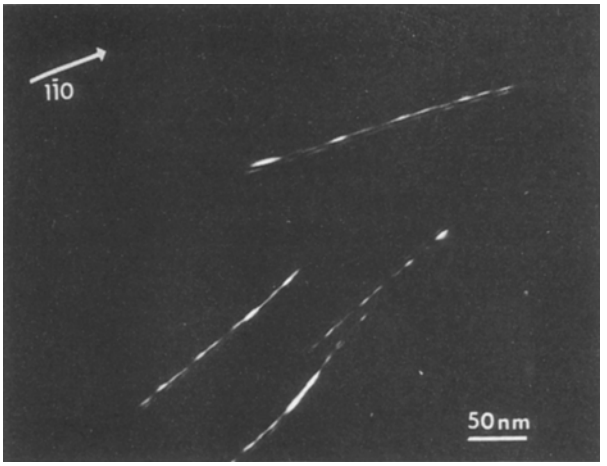

Figure 7 Weak-beam electron micrograph of a ⟨1 1 1⟩ APB (γ_1)-coupled pair in DO_3-structured Fe–34Al, strained in compression at room temperature. The spacing between the dislocations is ~ 5 nm. Diffraction vector as shown, $s > 0.2\,nm^{-1}$, $B \sim [1\,1\,1]$.

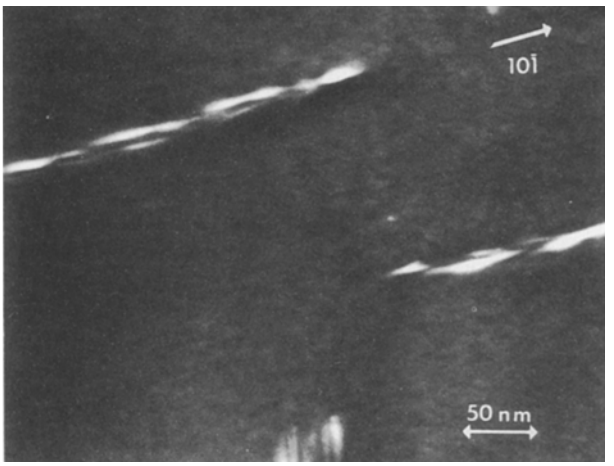

Figure 8 Weak-beam electron micrograph of a ⟨1 1 1⟩ APB (γ_1)-coupled pair in DO_3-structured Fe–28Al–6Cr, lightly rolled at room temperature. The spacing between the dislocations is ~ 8 nm. Diffraction vector as shown, $s > 0.2\,nm^{-1}$, $B \sim [1\,1\,1]$.

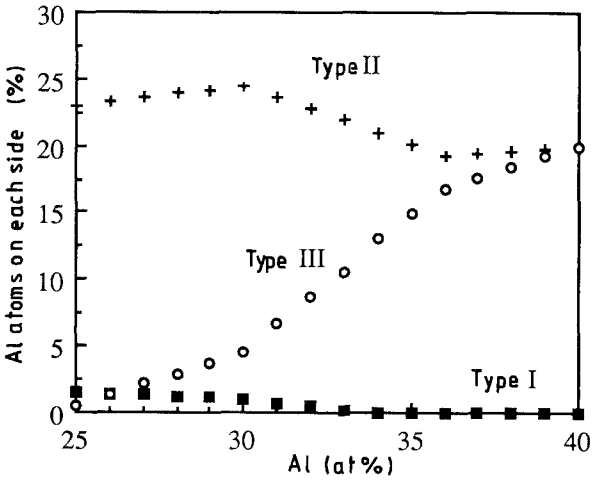

Figure 9 Distribution of aluminium atoms between lattice sites in Fe–Al alloys (after [15]). See Fig. 1b for the definition of the site types.

(γ_1) energy of ~ 79 mJ m^{-2} (Fig. 8). Again, no four-fold dislocations were observed.

4. Discussion

⟨0 0 1⟩ dislocations were not reported in a previous study of DO_3-structured Fe–34Al [10]. However, because the energetic driving force for the reaction, through which ⟨0 0 1⟩ dislocations are formed, is the reduction in APB energy [8], the density of ⟨0 0 1⟩ dislocations in Fe–34Al is low compared with more aluminium-rich alloys, where the APB energy is higher. That no four-fold dislocations were observed in this study is consistent with previous work [10] where it was suggested that the γ_2 energy was sufficiently low at this composition for the γ_1-coupled pairs to glide independently trailing an APB. However, because X-ray diffraction studies have suggested that Fe–34Al has little DO_3 character [15], it is probable that the APB (γ_2) pairs were never present. It is pertinent to note that the room-temperature mechanical properties of Fe–34Al, tested in both the B2 and the DO_3 conditions, were indistinguishable [19].

McKamey *et al.* [11] measured R_1 and R_2 in Fe–28Al to be 7 and 37 nm, respectively, and in Fe–28Al–4Cr to be 15 and 60 nm, respectively. Thus it is clear that the addition of 4% chromium decreased both γ_1 and γ_2. Furthermore, chromium additions to Fe–28Al increased room-temperature ductility and produced a change in fracture mode from transgranular cleavage to a mixed mode failure [11]. The increase in ductility was attributed to the ease of cross-slip with the increased separation of the partials. An additional mechanism may be that the chromium additions decrease the APB (γ_1) energy, and so reduce the driving force for ⟨0 0 1⟩ dislocation formation, and thus decrease the incidence of transgranular fracture [8].

In the present study, no four-fold dislocations were observed in Fe–28Al–6Cr, suggesting that the higher chromium additions further decreased the DO_3

character, i.e. decreased γ_2. However, R_1 was measured to be only ~ 8 nm, less than the value obtained for Fe–28Al–4Cr and consistent with a value of $\sim 79\ mJ\ m^{-2}$. Thus, it would seem that while small chromium additions (4%) reduce the B2 character (decreased γ_1), further additions of chromium (6%) increase the B2 character (at least compared to Fe–28Al–4Cr). The change in APB (γ_1) energy with chromium additions may be rationalized by considering the site occupancy of aluminium atoms in Fe–Al alloys containing between 25% and 40% aluminium [15] (Fig. 9). Between the stoichiometric Fe_3Al composition and Fe–30Al, the type II sites are almost totally filled with aluminium atoms, and the excess aluminium atoms occupy both type I and type III sites. But between 30% and 35% Al, the density of aluminium atoms on the type II sites decreases as the density of aluminium atoms on the type III sites increases. Clearly, this change in site occupancy between 30% and 35% Al will decrease the DO_3 character and increase the B2 character, that is, increase γ_1 and decrease γ_2. It has been determined that chromium atoms occupy the aluminium sublattice in iron-rich FeAl-based alloys [20, 21]. Thus, addition of chromium to DO_3Fe_3Al will affect the APB (γ_1) energy in two competing ways, chromium atoms will produce changes in bonding energy so decreasing the APB (γ_1) energy, but the presence of chromium atoms on type II and type III sites will decrease the number of iron antisite defects on these sites and so increase the APB (γ_1) energy. The effect of a large number of chromium atoms (6%) occupying the aluminium sublattice may be to increase γ_1 with respect to a smaller chromium concentration (4%) through the decreased density of the type II sites and the increased density of the type III sites.

5. Conclusions

Transmission electron microscope observations of both DO_3-structured Fe–34Al and Fe–28Al–6Cr lightly strained in compression at room temperature have led to the following conclusions.

1. The dislocation substructures of both alloys consisted of APB (γ_1)-coupled $\langle 1\,1\,1 \rangle$ dislocations, together with a low density of $\langle 0\,0\,1 \rangle$ dislocations.

2. Addition of 6% chromium to DO_3-structured Fe–28Al reduces the DO_3 character, but increases the B2 character.

Acknowledgements

The authors thank Dr F. D. Lemkey, United Technologies Research Center, for providing the ingots, and Mr D. J. Gaydosh and Dr J. D. Whittenberger, NASA-Lewis Research Center for extruding them. Drs C. G. McKamey and C. T. Liu are thanked for provision of the Fe–28Al–6Cr alloy. F. Liu and P. Nagpal are acknowledged for their assistance with specimen preparation. This work was supported by the Office of Basic Energy Sciences of the US Department of Energy through grant DE-FG02-87ER45311. The use of the Dartmouth College Electron Microscope Center is also acknowledged.

References

1. T. B. MASSALSKI (ed.), "Binary Phase Alloy Diagrams" (ASM, Metals Park OH, 1986) p. 112.
2. T. YAMAGATA and H. YOSHIDA, *Mater. Sci. Engng* **12** (1973) 95.
3. T. YAMAGATA, *Trans. Jpn Inst. Metals* **18** (1977) 715.
4. Y. UMAKOSHI and M. YAMAGUCHI, *Phil. Mag. A* **41** (1980) 573.
5. *Idem, ibid.* **44** (1981) 711.
6. M. G. MENDIRATTA, H.-M. KIM and H. A. LIPSITT, *Metall. Trans.* **15A** (1984) 395.
7. I. BAKER and D. J. GAYDOSH, *Mater. Sci. Engng* **96** (1987) 147.
8. P. R. MUNROE and I. BAKER, *Acta Metall.* **39** (1991) 1011.
9. M. J. MARCINKOWSKI and N. BROWN, *ibid.* **9** (1961) 764.
10. R. C. CRAWFORD and I. L. F. RAY, *Phil. Mag.* **35** (1977) 549.
11. C. G. McKAMEY, J. HORTON and C. T. LIU, *J. Mater. Res.* **4** (1989) 1156.
12. P. R. MUNROE and I. BAKER, *J. Mater. Sci.* **24** (1990) 4246.
13. I. BAKER and D. J. GAYDOSH, *Phys. Status Solidi.* **96** (1986) 185.
14. P. B. HIRSCH, A. HOWIE, R. B. NICHOLSON, D. W. PASHLEY and M. J. WHELAN, "Electron Microscopy of Thin Crystals" (R. E. Kreiger, Malabar FL, 1965) p. 181.
15. A. J. BRADLEY and A. H. JAY, *Proc. Roy. Soc.* **A139** (1932) 210.
16. H. J. LEAMY and F. X. KAYSER, *Phys. Status. Solidi* **34** (1969) 765.
17. P. R. MUNROE and I. BAKER, *Scripta Metall.* **23** (1989) 495.
18. A. HEAD, P. HUMBLE, L. M. CLAREBOROUGH, A. J. MORTON and C. T. FORWOOD, "Computed Electron Micrographs and Defect Identification" (North Holland, Amsterdam, 1973) p. 136.
19. I. BAKER, P. NAGPAL, F. LIU and P. R. MUNROE, *Acta Metall. Mater.* **39** (1991) 1637.
20. P. R. MUNROE and I. BAKER, in "Proceedings of the XIIth Electron Microscopy Congress", Seattle, August 1990, edited by G. W. Bailey (San Francisco Press, San Francisco, 1990) Vol. 2, p. 472.
21. *Idem, Scripta Metall. Mater.* **24** (1990) 2273.

Received 18 January
and accepted 7 June 1991